

Properties of $\text{Al}_2\text{O}_3\text{--Sm}_2\text{O}_3\text{--CeO}_2$ electrolyte

S. RAMESH¹, K. C. J. RAJU¹, C. V. REDDY²

1. School of Physics, University of Hyderabad, Hyderabad 500046, India;

2. Department of Physics, Osmania University, Hyderabad 500007, India

Received 25 October 2011; accepted 10 January 2012

Abstract: $\text{Ce}_{1-x}\text{Sm}_x\text{O}_2$ ($x=0, 0.1, 0.2$ and 0.3) and Sm-doped ceria+(2%–8%) Al_2O_3 were synthesized through sol–gel process followed by low temperature combustion. The synthesis, structure, densification, conductivity and thermal expansion were studied, and the structure and phase were confirmed by XRD. Dense ceramics were obtained through sintering the pellets at 1300 °C. 2% and 4% Al_2O_3 were added into $\text{Ce}_{0.8}\text{Sm}_{0.2}\text{O}_2$ to promote the densification at 1250 °C. The surface morphology of the sintered pellets was analyzed using SEM. A two-probe AC impedance spectroscopy was used to study the total ionic conductivity.

Key words: sol–gel process; XRD-rietveld; impedance spectroscopy; ionic conductivity; electrolyte; ceramics

1 Introduction

Solid oxide fuel cells (SOFCs) are used as electrochemical devices since they convert chemical energy into electrical energy. SOFCs have been attracted more attention because they provide clean, high and efficient electrical power. Yttria-stabilized zirconia (YSZ) is a standard electrolyte for solid oxide fuel cell applications. High operating temperatures (>1000 °C) are required to increase the ionic conductivity of YSZ. However, there are problems like thermal mismatch between cell components, chemical instability and selection of materials at such high operating temperatures [1–3]. Therefore, there is a strong motivation to search for new improved oxide-ion electrolytes at intermediate temperature (400–700 °C). In order to increase the applicability of electrolyte, it is essential to reduce the operating temperature.

Currently, in the search of advanced materials, CeO_2 is an alternate material doped with alkaline earth or rare earth materials. Generally, a single SOFC consists of anode, electrolyte and cathode materials in contact. However, the efficiency of the fuel cell depends on electrolyte materials. A good electrolyte material should have high density (over 98%), high ionic conductivity, low thermal expansion and negligible electronic conductivity. Classical solid-state method needs the sintering temperature in the range of 1500–1600 °C to

prepare dense ceramics and the main problems in this method are the lack of homogeneity in mixing materials and microstructure at such high sintering temperatures and the reduction from Ce^{4+} to Ce^{3+} . The reduction of ceria increases the electronic conductivity, which decreases the performance of the cell [4]. However, sintering temperature can be reduced by the selection of suitable method for material preparation.

Among various dopants, Sm-doped ceria (SDC) has been reported to have a high ionic conductivity [2]. Studies [5–11] show that co-doping could increase the ionic conductivity.

In the present study, SDC-based materials, $\text{Ce}_{0.9}\text{Sm}_{0.1}\text{O}_2$ (SDC10), $\text{Ce}_{0.8}\text{Sm}_{0.2}\text{O}_2$ (SDC20), $\text{Ce}_{0.7}\text{Sm}_{0.3}\text{O}_2$ (SDC30) and SDC20+(2%–8%) Al_2O_3 were prepared and characterized. The main aim is to investigate the effects of dopants on the crystal structure, and sintering temperature on densification, electrical properties and thermal expansion of doped ceria materials.

2 Experimental

The polycrystalline samples with general formula $\text{Ce}_{1-x}\text{Sm}_x\text{O}_2$ (0, 0.1, 0.2 and 0.3), SDC20+(2%–8%) Al_2O_3 were synthesized through sol–gel process followed by low temperature combustion to make different metal ions mixed more homogeneously. High purity cerium nitrate hexahydrate ($\text{Ce}(\text{NO}_3)_3 \cdot 6\text{H}_2\text{O}$)

($\geq 99.9\%$ Sigma-Aldrich), samarium nitrate hexahydrate ($\text{Sm}(\text{NO}_3)_3 \cdot 6\text{H}_2\text{O}$) ($\geq 99.9\%$ Sigma-Aldrich) and Al_2O_3 were used as starting materials. Nitric acid and Al_2O_3 were converted into aluminum nitrate. Stoichiometric amounts of Ce, Sm and Al nitrates were dissolved in deionized water under continuously stirring in a beaker. Citric acid was added to the solution in 1:1 molar ratio and then ammonium hydroxide was added drop by drop to the solution to adjust $\text{pH} \approx 7$. The transparent solution was stirred at 40°C until a thick homogeneous solution was formed. Ethylene glycol was added to the solution in the molar ratio of 1:1.2 and heated at 40°C until a brownish sponge type viscous gel was formed. Afterward, the gel was placed in a burner, then auto ignition was completed in a few seconds, giving rise to a light yellow colored ash, which was calcined at 600°C for 4 h. The resultant ash was grounded in an agate mortar to get fine homogeneous powders.

Further the powders were pressed uni-axially with the help of hydraulic press under a continuous pressure of 20 MPa for 5 min into circular pellets using a stainless steel die with dimensions of $d10\text{ mm} \times 2\text{ mm}$ and then the green pellets were sintered in air at $1250\text{--}1300^\circ\text{C}$ for 10 h at a programmed heating rate of $5^\circ\text{C}/\text{min}$. The densities of the sintered samples were measured in water using the Archimedes method and the calculated densities of sintered samples were more than 93% of the theoretical density.

The X-ray diffraction patterns of the samples were obtained by Bruker-D8-Advanced using Cu K_α radiation. The lattice parameters were calculated using Fullprof software. The sintered pellets were polished, thermally etched and gold coated for microstructure analysis using a scanning electron microscope (FE-SEM) equipped with an energy dispersive X-ray spectrometer (EDX) analyzer.

The AC impedance spectra of the samples were recorded using Agilent precision impedance analyzer (4294 A) as a function of temperature ($300\text{--}700^\circ\text{C}$) in air in a measuring frequency range from 40 Hz to 1 MHz. Silver paste was brushed to each side of the samples, which was subsequently dried at 600°C for 20 min, producing solid silver electrode on both sides of the pellet. The thermal expansion measurements were carried out with Netzsch push-rod dilatometer (DIL; Model Netzsch DIL 402 PC, Germany) at a constant heating rate of $5^\circ\text{C}/\text{min}$ in the temperature range from 30 to 1000°C .

3 Results and discussion

3.1 Structure analysis

Figure 1(a) shows the XRD patterns of the $\text{Ce}_{1-x}\text{Sm}_x\text{O}_2$ powders. It can be seen from Fig. 1(a) that

powders contain only a cubic structure [12] with the space group $Fm\bar{3}m$ (JCPDS powder diffraction File No. 34–0394). Figure 1(b) shows the XRD patterns of SDC20+(2%–8%) Al_2O_3 system. It can be seen from Fig. 1(b) that there is an extra peak. This indicates the dissolution limit in CeO_2 solid solution. Table 1 lists the lattice parameters of the samples. The introduction of Sm^{3+} into Ce^{4+} can cause a small shift in the ceria peaks. This shift is an indicative of a change in the lattice parameters. This is due to the difference in ionic radii of Ce^{4+} (0.097 nm), Sm^{3+} (0.109 nm) and Al^{3+} (0.057 nm) [13] in an oxide solid solution. It can be observed from Table 1 that the lattice parameters decrease slightly

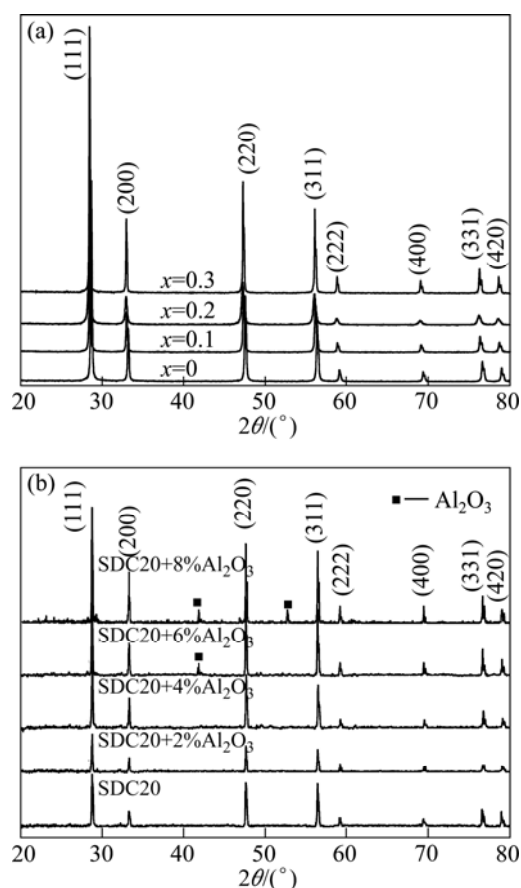


Fig. 1 XRD patterns of $\text{Ce}_{1-x}\text{Sm}_x\text{O}_2$ system (a) and SDC20+(2%–8%) Al_2O_3 (b)

Table 1 Physical properties of doped ceria

Composition	Structure	Lattice parameter/ \AA	Relative density/%
SDC10 ($\text{Ce}_{0.9}\text{Sm}_{0.1}\text{O}_2$)	Cubic	5.4248	93.2
SDC20 ($\text{Ce}_{0.8}\text{Sm}_{0.2}\text{O}_2$)	Cubic	5.4331	96.1
SDC30 ($\text{Ce}_{0.7}\text{Sm}_{0.3}\text{O}_2$)	Cubic	5.4457	93.3
SDC20+2% Al_2O_3	Cubic	5.4312	98.1
SDC20+4% Al_2O_3	Cubic	5.4302	96.8
SDC20+6% Al_2O_3	Cubic	5.4330	95.0
SDC20+8% Al_2O_3	Cubic	5.4330	95.5

compared with those of SDC20 when (2%–4%) Al_2O_3 is doped into SDC 20. This is due to the difference in ionic radii of Ce^{4+} (0.097 nm), Sm^{3+} (0.109 nm) and Al^{3+} (0.057 nm), whereas there is no change in lattice parameter when (6%–8%) Al_2O_3 is doped into SDC 20 (see Fig. 2). This is due to the extra peaks observed in the XRD patterns.

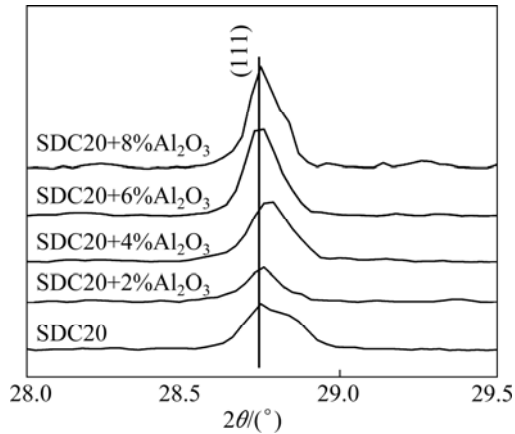


Fig. 2 Shift in 2θ of SDC20+(2%–8%) Al_2O_3

Figure 3 shows the Rietveld refinement of SDC20+2% Al_2O_3 using Fullprof software. Rietveld parameters R_p (profile parameter), R_{wp} (weighted profile parameter), R_{exp} (expected parameter) and χ^2 (reduced chi-square) are 4.05, 6.20, 5.87 and 0.895, respectively and the goodness of fit (GOF) is 1.052.

Figures 4–7 show the SEM images of $\text{Ce}_{1-x}\text{Sm}_x\text{O}_2$

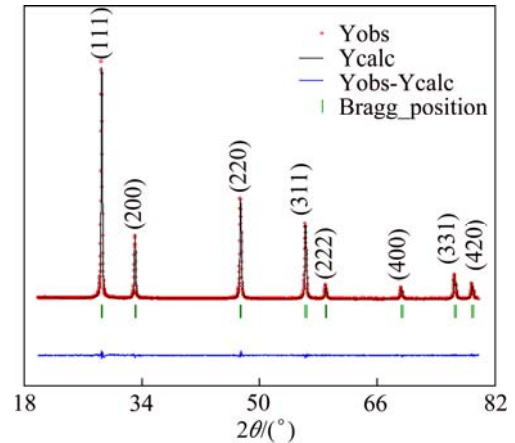


Fig. 3 Rietveld refinement of SDC20+2% Al_2O_3

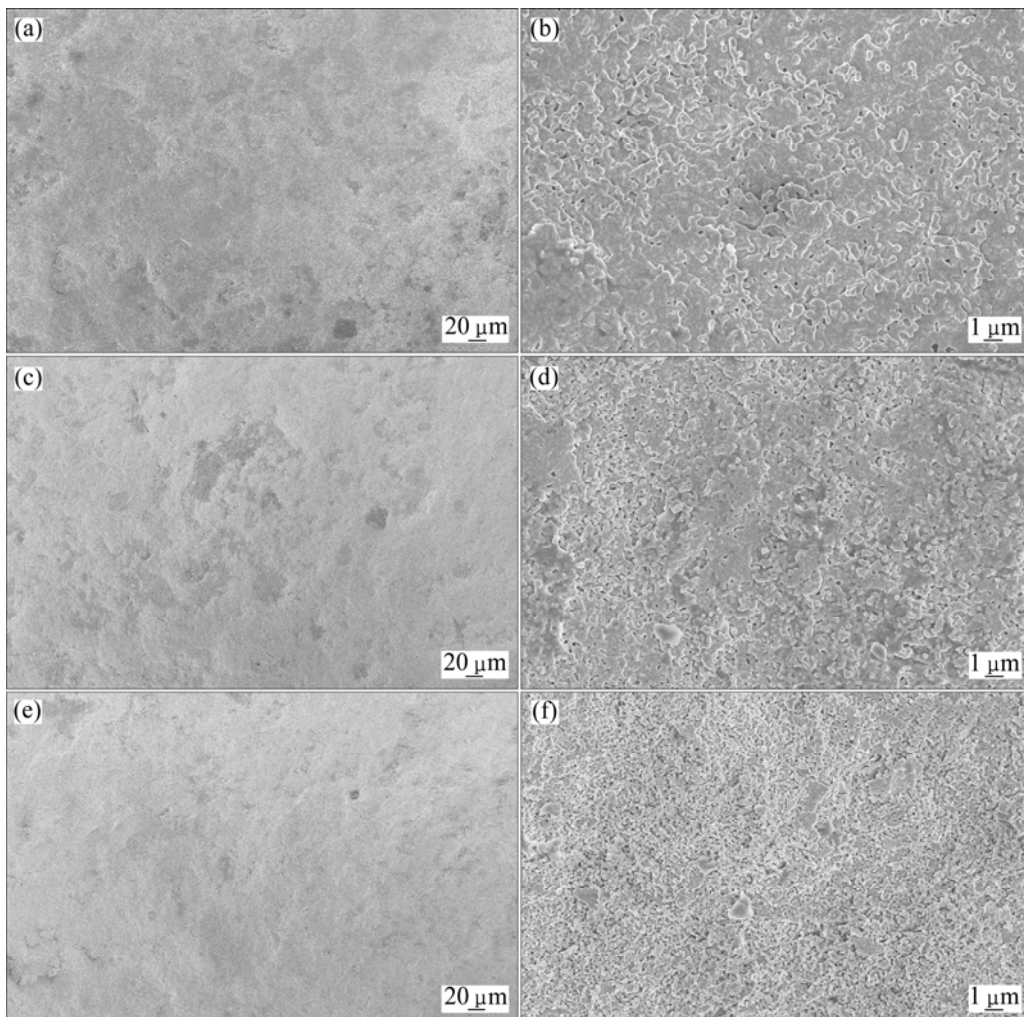


Fig. 4 SEM images of SDC10 sintered at different temperatures: (a), (b) 1300 °C; (c), (d) 1200 °C; (e), (f) 1100 °C

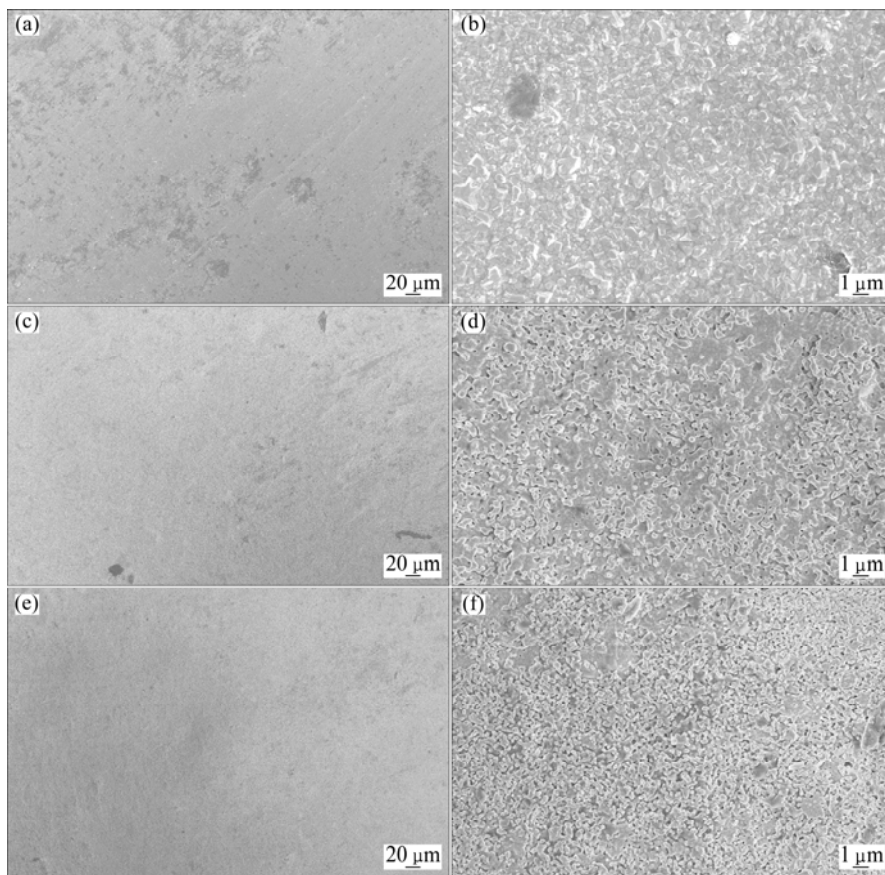


Fig. 5 SEM images of SDC20 sintered at different temperatures: (a), (b) 1300 °C; (c), (d) 1200 °C; (e), (f) 1100 °C

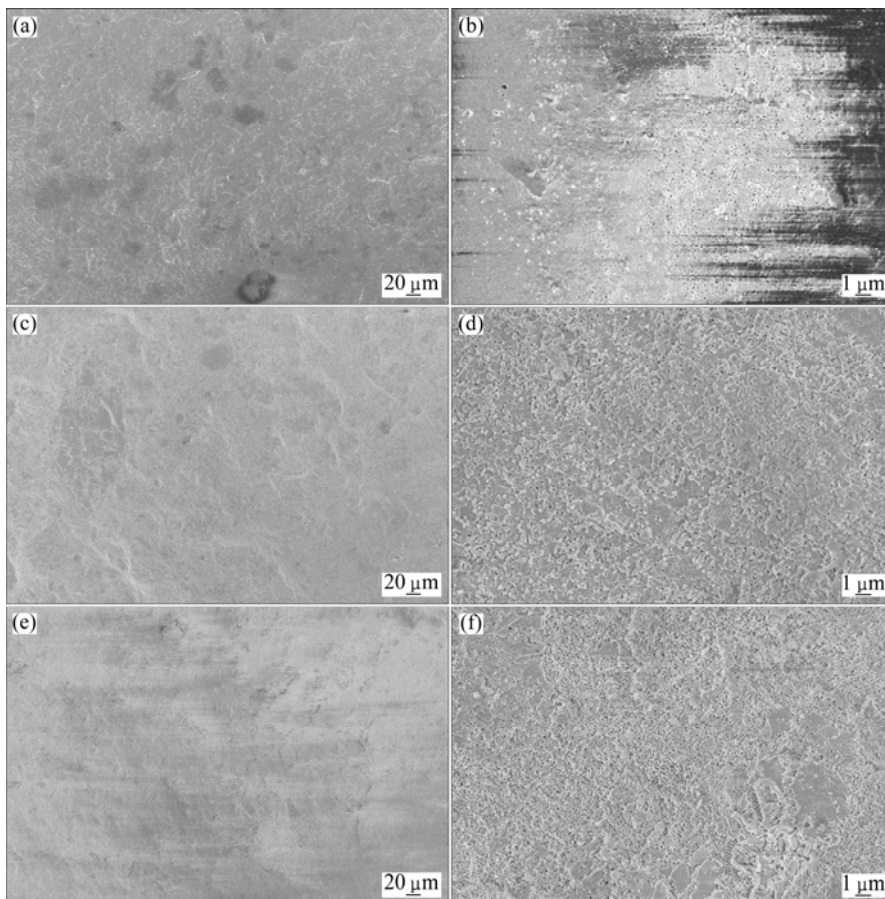


Fig. 6 SEM images of SDC30 sintered at different temperatures: (a), (b) 1300 °C; (c), (d) 1200 °C; (e), (f) 1100 °C

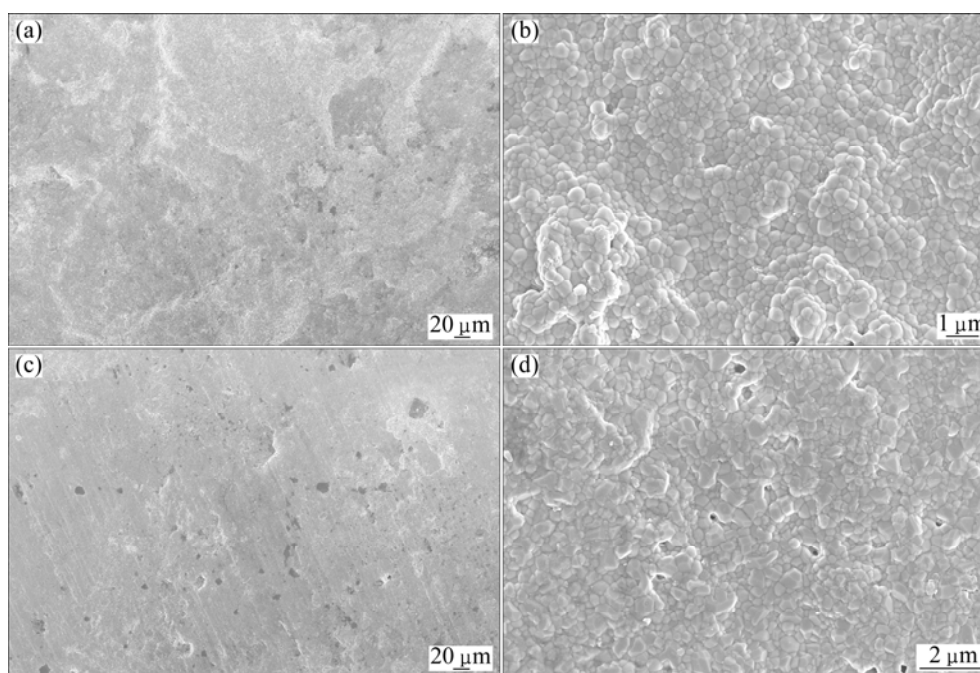


Fig. 7 SEM images of SDC20+2%Al₂O₃ (a, b) and SDC20+4%Al₂O₃ (c, d) sintered at 1250 °C

and SDC20+(2%–4%) Al₂O₃ samples. It is very clear that the surface of the samples is high dense at 1300 °C for (SDC20) Ce_{0.8}Sm_{0.2}O₂, whereas other SEM images show some closed pores. This is in good agreement with the relative density of the test samples. It is observed from Figs. 4–6 that the pores decrease with the increase in temperature. In the case of SDC20, these pores are not present while in the case of SDC10, more pores are observed. Further, it is noticed that the addition of (2%–4%) Al₂O₃ into SDC20 promotes the densification at lower sintering temperature (1250 °C). The SDC10 and SDC30 samples were sintered at 1300 °C to obtain relative density over 93% (Table 1) and SDC20+(2%–8%)Al₂O₃ samples were sintered at 1250 °C for 10 h to obtain relative density over 95%. The SDC20+2%Al₂O₃ sample shows good densification (over 98%). Also, SDC20+4%Al₂O₃ sample shows good densification (Fig. 7(b) and Table 1) and it can be seen that some closed pores are present on the sample surface. This indicates that the addition of Al₂O₃ into SDC20 acts as sintering aid and increases the density without affecting the structure. Further, the addition of (6%–8%) Al₂O₃ increases the density of SDC20 and affects the structure, as shown in Fig. 1(a), namely, secondary phase is formed. The SDC20+2%Al₂O₃ sample was sintered above 1250 °C and it is observed that there is a decrease in the relative density.

High density is achieved at relatively low temperatures (1250–1300 °C) by sol–gel process using low temperature combustion in comparison with the classical solid state reaction method, where temperature higher than 1500–1600 °C is needed to attain a highly

dense ceramics of SDC [14–17]. Further, it was reported that the different sintering aids like Fe₂O₃, Al₂O₃, ZnO and CuO can be employed to promote the densification and sintered over 1375 °C to obtain high dense ceramics [17, 18–22]. If the synthesized powder particle size is not small enough, then high sintering temperature is needed to obtain dense ceramics. Due to this fact in the present study, low temperature (40 °C) is used to burn the gel to get smaller size particles and it is observed that the synthesized powder size is changed with combustion temperature. This indicates that the samples prepared by sol–gel process followed by low temperature combustion could decrease the sintering temperatures below or at 1300 °C. In the case of SDC20, the same procedure was applied, but the samples were sintered at 1300 °C to get high dense ceramics, whereas in the case of SDC20 with Al₂O₃ addition, the samples were sintered at 1250 °C. This clearly indicates that Al promotes the densification of SDC20.

Figure 8 shows the energy dispersive spectra of SDC20 and SDC20+(2%–8%)Al₂O₃ samples. It is noticed that the compositions are in accordance with stoichiometry calculations. Also, smaller dopant percentage (in the case of 2%Al₂O₃) and all the composition elements are detected by EDX. It is noticed that no other extra elements are present.

3.2 Impedance spectroscopy

AC impedance spectroscopy is an important tool to study the grain, grain boundary and electrode contribution to the overall ionic conductivity. Figures 9(a) and (b) show the Nyquist plots of SDC20 and SDC20+

2%Al₂O₃ ceramic samples, respectively. Complete two depressed semi-circles and a part of arc are clearly seen. In this case, equivalent circuit grain resistance-(resistance-constant phase element)_{gb}-(resistance-constant phase element)_{electrode} is used to fit the impedance data to calculate grain (R_g) and grain boundary (R_{gb}) resistance. After 450 °C, the grain arc is not well resolved due to the decrease in relaxation time and it shifts towards the higher frequency region exceeding the equipment limit (higher frequencies are required to observe grain contribution). The use of

simple capacitor is not sufficient to model the electrical response of the materials due to the depression of arcs in some cases. For this reason, a constant phase element (CPE) was used to fit the results [23]. The main contribution of the conductivity of ceria-based compounds in air is the ionic conductivity and the contribution of the electronic conductivity is negligible [2,12,23]. In the present investigation, the measured conductivity is treated as oxide ion conductivity. It is noticed from Figs. 9(a) and (b) that the total resistance decreases when 2% Al₂O₃ is doped into SDC20.

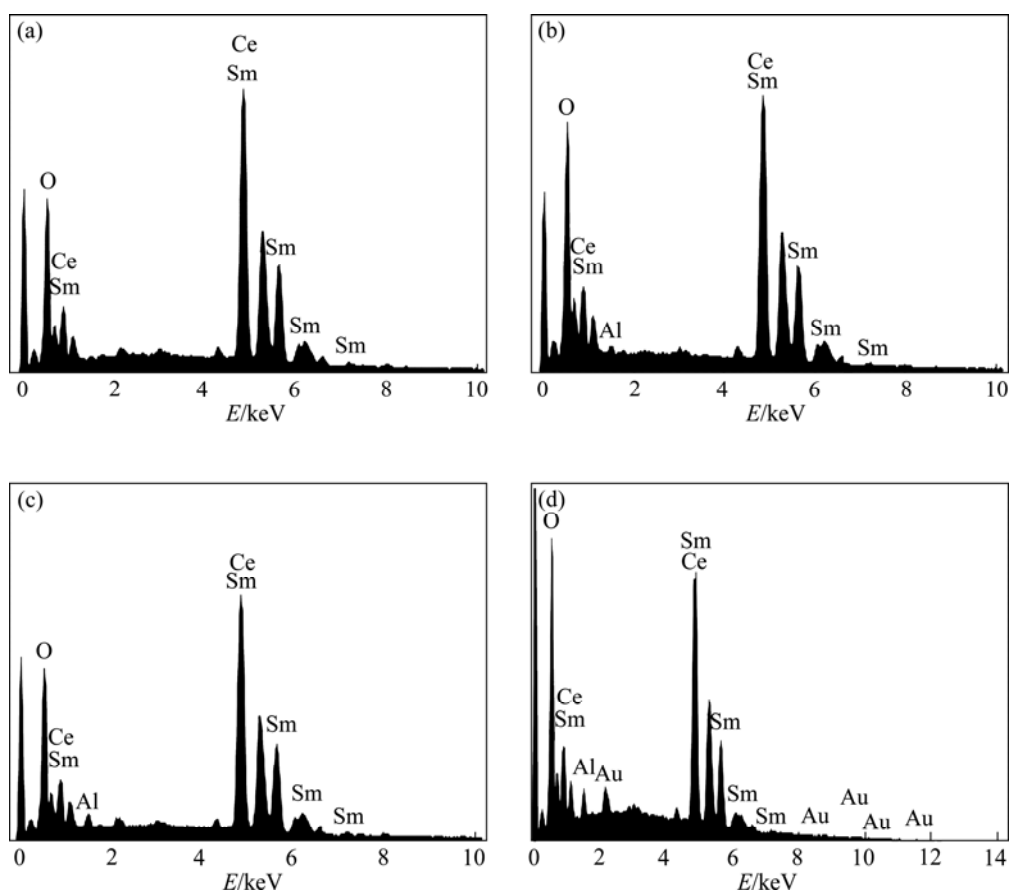


Fig. 8 EDX analyses of doped ceria samples: (a) SDC20; (b) SDC20+2%Al₂O₃; (c) SDC20+4%Al₂O₃; (d) SDC20+8%Al₂O₃

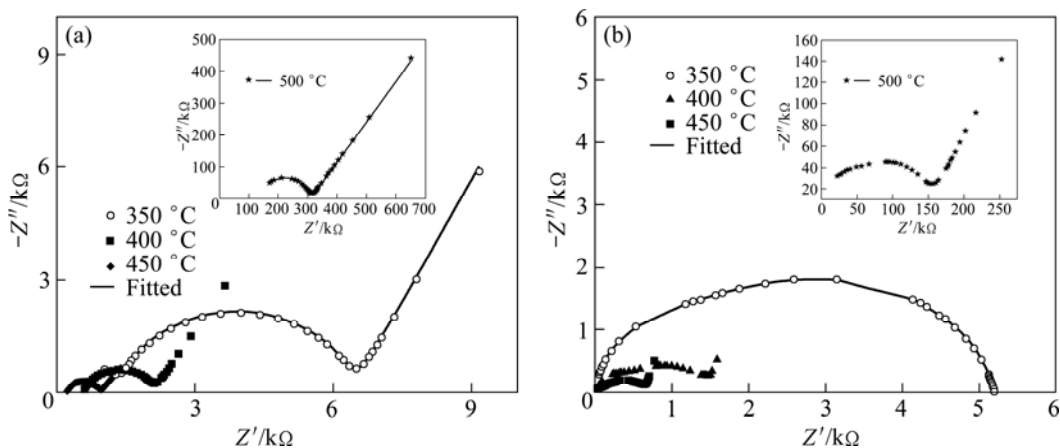


Fig. 9 Nyquist plots spectra of SDC20 (a) and SDC20+2%Al₂O₃ (b)

3.3 Total ionic conductivity

The total resistance (R_t) from Fig. 9 in terms of grain (R_g) and grain boundary resistance (R_{gb}) are given by:

$$R_t = R_g + R_{gb} \quad (1)$$

The total ionic conductivity (σ_t) is then calculated using total resistance (R_t), thickness (l) and cross-section area (A) using the following equation:

$$\sigma_t = \frac{l}{R_t A} \quad (2)$$

The activation energy for conduction is obtained by plotting the total ionic conductivity data in the Arrhenius relation for thermally activated conduction. It is calculated as:

$$\sigma T = \sigma_0 \exp\left(-\frac{E_a}{kT}\right) \quad (3)$$

where E_a is the activation energy for conduction; T is the thermodynamic temperature; k is the Boltzmann's constant; and σ_0 is a pre-exponential factor.

Figure 10 shows the Arrhenius plots of the total ionic conductivity for doped ceria ceramics. It is noticed that the total ionic conductivity changes with the addition of Al_2O_3 . The conductivity increases up to dopant concentration of 2% Al_2O_3 and then it decreases. Also, it can be seen that the conductivity difference is larger in lower temperature region than that in the higher temperature region for all the samples. It can be seen from Fig. 10 that the SDC20+2% Al_2O_3 sample shows higher conductivity with lower activation energy (0.82 eV) than SDC20 (0.86 eV). The 6% and 8% Al_2O_3 doped SDC20 samples do not show any further improvement in the ionic conductivity due to the formation of second phase Al_2O_3 , which decreases the conductivity. Further, the total ionic conductivity of SDC20 is higher than that of the SDC10 or SDC30.

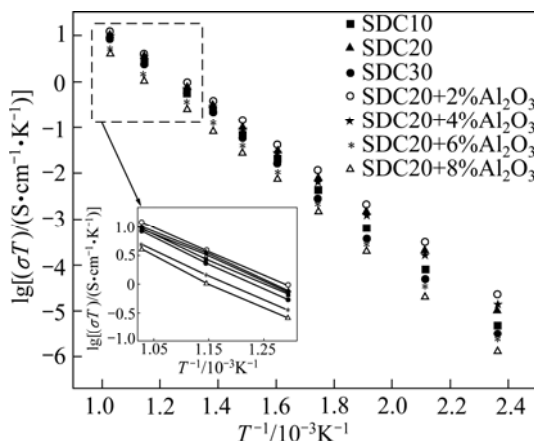


Fig. 10 Arrhenius plots of doped ceria samples

Oxide vacancies ($\text{V}_\text{O}^{\circ\circ}$) may be created in CeO_2 by doping Sm_2O_3 [1,2]. These equations are written in Kroger-Vink notation [2]. The lattice mismatch between Al^{3+} (0.057 nm) and Ce^{4+} (0.097 nm) is higher than that between Sm^{3+} (0.1079 nm) and Ce^{4+} (0.097 nm). Also, the electro-static attraction between Al–Ce and $\text{V}_\text{O}^{\circ\circ}$ is stronger than that between Sm–Ce and $\text{V}_\text{O}^{\circ\circ}$. Hence, the defect association between Al–Ce and $\text{V}_\text{O}^{\circ\circ}$ is expected to be more easily determinable than that between Sm–Ce and $\text{V}_\text{O}^{\circ\circ}$. Al^{3+} ions attract $\text{V}_\text{O}^{\circ\circ}$ to form the defect complex, which decreases the conductivity. The second-phase Al_2O_3 also decreases the electrochemical properties when the Al_2O_3 content in SPC20 exceeds 6% [17].

3.4 Thermal expansion coefficient

Figure 11 shows the thermal expansion curves of doped ceria in the temperature range from 30 to 1000 °C in air. From Fig. 11, it is noticed that the thermal expansion curves are linear. The thermal expansion depends on the electrostatic forces within the lattice which is up to the concentration of positive and negative charges and their distances within the lattice [6]. The

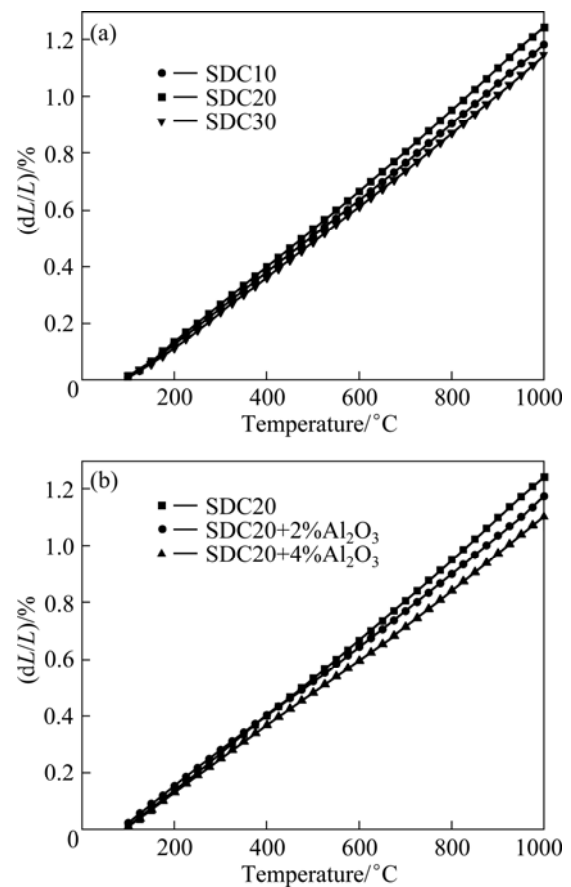


Fig. 11 Thermal expansion curves of $\text{Ce}_{1-x}\text{Sm}_x\text{O}_2$ system (a) and SDC20+(2%–4%) Al_2O_3 (b)

thermal expansivity (TE) can be calculated from the expansion curves using the following expression as:

$$\alpha_{\Delta T} = \frac{dL}{L\Delta T} \quad (4)$$

where $\alpha_{\Delta T}$ is the average of TE in the temperature range of ΔT , dL is the change of the sample length in ΔT and L is the original length of the sample.

The solid oxide fuel cell mainly consists of an anode, cathode, solid electrolyte and inter-connect and it can be regarded as a typical example of composite materials. When such composite materials are used at high temperatures, the thermal expansion should be matched between them; otherwise, micro-cracks would occur during heating cycles. The calculated TEs are listed in Table 2. It is clear that the TEs decrease with the addition of Al_2O_3 to SDC20. It is noticed that the change of TE is very small. The results are in good agreement with the reported values [6]. Further work is in progress to construct the solid oxide fuel cell and to study the application of this electrolyte.

Table 2 Thermal expansivity of doped ceria

Composition	TE/ $10^{-6} \text{ }^\circ\text{C}^{-1}$				
	600 °C	700 °C	800 °C	900 °C	1000 °C
SDC10	10.89	11.36	11.65	11.94	12.10
SDC20	11.57	11.92	12.25	12.55	12.73
SDC30	10.65	10.92	11.23	11.47	11.73
SDC20+2% Al_2O_3	11.18	11.37	11.60	11.81	12.03
SDC20+4% Al_2O_3	10.35	10.56	10.85	11.10	11.30

4 Conclusions

1) Al and Sm-doped ceria samples are successfully prepared through sol-gel process followed by low temperature combustion. The effect of Al_2O_3 on density, structure and total ionic conductivity is investigated.

2) Dense ceramics are obtained by sintering the pellets between 1250 and 1300 °C and the results are consistent with the SEM analysis.

3) Addition of Al_2O_3 into SDC20 increases the densification and decreases the sintering temperature to 1250 °C. Dissolution limit restricts the addition of Al_2O_3 above 4%. Secondary phase is observed when above 4% Al_2O_3 is doped into SDC20. 2% addition of Al_2O_3 decreases the total resistance of SDC20. Improved total ionic conductivity and minimum activation energy are observed in the SDC20+2% Al_2O_3 composition.

Acknowledgement

Dr. S. RAMESH would thank UGC-DSKPDF for funding.

References

- [1] KILNER J A. Fast oxygen transport in acceptor doped oxides [J]. *Solid State Ionics*, 2000, 129(1–4): 13–23.
- [2] INABA H, TAGAWA H. Ceria based solid electrolytes [J]. *Solid State Ionics*, 1996, 83(1–2): 1–16.
- [3] NEILSEN J, HAGEN A, LIU Y L. Effect of cathode gas humidification on performance and durability of solid oxide fuel cells [J]. *Solid State Ionics*, 2010, 181(11–12): 517–524.
- [4] MOURE A, MOURE C, TARTAJ J. A significant improvement of the processing and electric properties of CeO_2 co-doped with Ca and Sm by mechano-synthesis [J]. *J Power Sources*, 2011, 196(24): 10543–10549.
- [5] LUBKE S, WEIMHOFER H D. Electronic conductivity of Gd-doped ceria with additional Pr-doping [J] *Solid State Ionics*, 1999, 117(3–4): 229–243.
- [6] RAMESH S, KUMAR V P, KISTAIAH P, REDDY C V. Preparation, characterization and thermoelectrical properties of co-doped $\text{Ce}_{0.8-x}\text{Sm}_x\text{O}_{2-\delta}$ materials [J]. *Solid State Ionics*, 2010, 181(1–2): 86–91.
- [7] LIU Y Y, PAN W, LI B, WEI X. Citric-nitrate combustion synthesis and electrical conductivity of the Sm^{3+} and Nd^{3+} co-doped ceria electrolyte [J]. *J Am Ceram Soc*, 2008, 91(12): 3926–3930.
- [8] RAMESH S, REDDY C V. Electrical properties of co-doped $\text{Ce}_{0.8-x}\text{Gd}_x\text{O}_{2-\delta}$ electrolyte [J]. *Acta Physica Polonica A*, 2009, 115(5): 909–913.
- [9] KIM N, KIM B. H, LEE D. Effect of co-dopant addition on properties of gadolinia-doped ceria electrolyte [J]. *J Power Sources*, 2000, 90(2): 139–143.
- [10] WANG F Y, WAN B Z, CHENG S. Study on Gd^{3+} and Sm^{3+} co-doped ceria-based electrolytes [J]. *J Solid State Electrochem*, 2005, 9(3): 168–173.
- [11] WANG F Y, CHEN S, WANG Q, YU S, CHENG S. Study on Gd and Mg co-doped ceria electrolyte for intermediate temperature solid oxide fuel cells [J]. *Catal Today*, 2004, 97(2–3): 189–194.
- [12] RAMESH S, JAMES R K C. Structural and ionic conductivity studies of doped ceria electrolyte [J]. *Electrochemical and Solid State Letters B*, 2012, 15(3): 24–26.
- [13] SHANNON R D. Revised effective ionic radii and systematic studies of interatomic distances in halides and chalcogenides [J]. *Acta Cryst A*, 1976, 32(5): 751–767.
- [14] ZHAN Z, WEN T L, TU H, LU Z Y. AC impedance investigation of samarium-doped ceria [J]. *J Electrochem Soc A*, 2001, 148(5): 427–432.
- [15] ISHIDA T, IGUCHI F, SATO K, HASHIDA T, YUGAMI H. Fracture properties of $(\text{CeO}_2)_{1-x}(\text{RO}_{1.5})_x$ (R=Y, Gd, and Sm; $x=0.02-0.20$) ceramics [J]. *Solid State Ionics*, 2005, 176(31–34): 2417–2421.
- [16] OMER S, WACHSMAN E D, NINO J C. Higher conductivity Sm^{3+} and Nd^{3+} co-doped ceria-based electrolyte materials [J]. *Solid State Ionics*, 2008, 178(37–38): 1890–1897.
- [17] ZHENG Y, ZHOU M, GE L, LI S, CHEN H, GUO L. Effect of Fe_2O_3 on Sm-doped ceria system solid electrolyte for IT-SOFCs [J]. *J Alloys Compounds*, 2011, 509(2): 546–550.
- [18] YOUNG JIN KANG, HEE J P, GYEONG M C. The effect of grain size on the low-temperature electrical conductivity of doped CeO_2 [J]. *Solid State Ionics*, 2008, 179(27–32): 1602–1605.
- [19] ZHANG T S, ZENG Z Q, HUANG H T, HING P, KILNER J. Effect of alumina addition on the electrical and mechanical properties of $\text{Ce}_{0.8}\text{Gd}_{0.2}\text{O}_{2-\delta}$ ceramics [J]. *Materials Letters*, 2002, 57(1): 124–129.
- [20] GAO L, ZHOU M, ZHENG Y F, GU H T, CHEN H, GUO L C. Effect of zinc oxide on yttria doped ceria [J]. *J Power Sources*, 2010, 195(10): 3130–3134.

- [21] JINKANG Y, CHOI G M. The effect of alumina and Cu addition on the electrical properties and the SOFC performance of Gd-doped CeO₂ electrolyte [J]. Solid State Ionics, 2009, 180(11–13): 886–890.
- [22] KIM H N, PARK H J, CHOI G M. The effect of alumina addition on the electrical conductivity of Gd-doped ceria [J]. J Electroceram, 2006, 17(2–4): 793–798.
- [23] RAMESH S, JAMES R K C. Preparation and characterization of Ce_{1-x}(Gd_{0.5}Pr_{0.5})_xO₂ electrolyte for IT-SOFCs [J]. Int J Hydrogen Energy, 2012, 37(13): 10311–10317.

Al₂O₃-Sm₂O₃-CeO₂ 电解质的性能

S. RAMESH¹, K. C. J. RAJU¹, C. V. REDDY²

1. School of Physics, University of Hyderabad, Hyderabad 500046, India;

2. Department of Physics, Osmania University, Hyderabad 500007, India

摘要: 采用溶胶-凝胶法和低温燃烧技术制备 Ce_{1-x}Sm_xO₂ (x=0, 0.1, 0.2, 0.3)和掺杂 Sm 和(2%–8%)Al₂O₃ 的二氧化铈; 研究其合成、结构、致密化、导电性和热膨胀等性能, 并利用 XRD 研究其结构和相组成。结果表明, 于 1300 °C 烧结球团, 获得致密的陶瓷, 于 1250 °C 在 Ce_{0.8}Sm_{0.2}O_{0.2} 中加入 2% 和 4% 的 Al₂O₃ 以促进烧结。利用扫描电子显微镜观察烧结后球团的表面形貌, 使用双探针交流阻抗谱研究总离子电导率。

关键词: 溶胶-凝胶法; XRD-Rietveld; 阻抗法; 离子电导率; 电解质; 陶瓷

(Edited by FANG Jing-hua)